EUROPEAN ORGANIZATION FOR NUCLEAR RESEARCH

PA05-056

Measurement of $|V_{\rm cb}|$ and form factors in $\overline{\rm B}^0 \to {\rm D}^{*+}\ell^-\overline{\nu_\ell}$ and $\overline{\rm B}^0 \to {\rm D}^{+}\ell^-\overline{\nu_\ell}$ decays

The ALEPH Collaboration

Abstract

Two samples of exclusive semileptonic decays, 579 ± 30 $\overline{\rm B}^0 \to {\rm D}^{*+}\ell^-\overline{\nu_\ell}$ events and 266 ± 24 $\overline{\rm B}^0 \to {\rm D}^{+}\ell^-\overline{\nu_\ell}$ events, are selected from approximately 3.9 million hadronic Z decays collected by the ALEPH detector at LEP from 1991 to 1995. The reconstructed differential decay rate $d\Gamma/d\omega$ of each sample is fitted, yielding a measurement of the product of the hadronic form factor $\mathcal{F}(\omega = 1)$ at zero recoil of the ${\rm D}^{(*)+}$ meson and the CKM matrix element $|V_{\rm cb}|$, $\mathcal{F}_{\rm D^{*+}}(1)|V_{\rm cb}| = (30.6 \pm 1.8_{\rm stat} \pm 2.0_{\rm syst})\ 10^{-3}$ and $\mathcal{F}_{\rm D^{+}}(1)|V_{\rm cb}| = (28.8 \pm 6.7_{\rm stat} \pm 6.9_{\rm syst})\ 10^{-3}$. The ratio of the form factors $\mathcal{F}_{\rm D^{+}}(1)$ and $\mathcal{F}_{\rm D^{*+}}(1)$ is measured to be $\mathcal{F}_{\rm D^{+}}(1)/\mathcal{F}_{\rm D^{*+}}(1) = 0.94 \pm 0.23_{\rm stat} \pm 0.23_{\rm syst}$. A value of $|V_{\rm cb}|$ is extracted from the simultaneous fit of the $d\Gamma/d\omega$ distributions of the two samples, using theoretical constraints on the slope and curvature of the hadronic form factors and their calculated values at $\omega = 1$, with the result $|V_{\rm cb}| = (33.4 \pm 2.0_{\rm stat} \pm 2.3_{\rm syst} \pm 1.3_{\rm th})\ 10^{-3}$. The branching fractions ${\rm Br}(\overline{\rm B}^0 \to {\rm D}^{*+}\ell^-\overline{\nu_\ell}) = (5.14 \pm 0.24_{\rm stat} \pm 0.48_{\rm syst})\%$ and ${\rm Br}(\overline{\rm B}^0 \to {\rm D}^{+}\ell^-\overline{\nu_\ell}) = (2.41 \pm 0.21_{\rm stat} \pm 0.44_{\rm syst})\%$ are measured from the two integrated spectra.

Paper contributed to Warsaw Conference, July 1996

1 Introduction

The Heavy Quark Effective Theory (HQET) is a well established theoretical framework in which heavy hadrons properties and related observables can be studied reliably in a well defined limit of QCD [1]. Heavy quark symmetry relates all hadronic form factors in B semileptonic decays to a single universal form factor, the Isgur-Wise function and fixes its normalisation at zero recoil. This property allows for an almost model-independent determination of the CKM matrix element $|V_{\rm cb}|$ from the study of exclusive semileptonic B meson decays close to zero recoil of the charm meson.

To date all measurements of $|V_{\rm cb}|$ based on exclusive semileptonic B decays have been performed from the differential decay rate of $\overline{\rm B}^0 \to {\rm D}^{*+}\ell^-\overline{\nu_\ell}$ [2, 3, 4, 5]. In the limit of zero lepton mass, the differential decay rate is:

$$\frac{d\Gamma_{\rm D^{*+}}}{d\omega}(\omega) \;=\; \frac{{\rm G_F^2}}{48\pi^3} m^3_{\rm D^{*+}} (m_{\rm B^0} - m_{\rm D^{*+}})^2 {\rm K}(\omega)(\omega^2-1)^{1/2} \mathcal{F}^2_{\rm D^{*+}}(\omega) |V_{\rm cb}|^2 \;, \qquad (1)$$

where ω is the scalar product of the two mesons four-velocities $\omega = \frac{m^2_{\rm B^0}+m^2_{\rm D^{(*)+}}-q^2}{2m_{\rm B^0}m_{\rm D^{(*)+}}}$, q^2 being the mass of the $\ell\nu_\ell$ system. ${\rm K}(\omega)$ is a known kinematicfunction and $\mathcal{F}_{\rm D^{*+}}(\omega)$ is the hadronic form factor of the decay $\overline{\rm B}^0 \to {\rm D}^{*+}\ell^-\overline{\nu_\ell}$.

The strategy used [6] is to measure $\mathcal{F}_{\rm D^{*+}}(1)|V_{\rm cb}|$ from $d\Gamma/d\omega$ by extrapolation to $\omega = 1$ (point of zero recoil of the $\rm D^{*+}$ meson) and to determine $|V_{\rm cb}|$ using the theoretical prediction of $\mathcal{F}_{\rm D^{*+}}(1)$. The theoretical uncertainty in this determination is of order 3% [7].

The semileptonic decay $\overline{\rm B}^0 \to {\rm D}^{+}\ell^-\overline{\nu_\ell}$ can also be used to measure $|V_{\rm cb}|$. Experimentally this decay channel is more difficult to tag for reasons that will become apparent. In the limit of zero lepton mass the differential decay rate of $\overline{\rm B}^0 \to {\rm D}^{+}\ell^-\overline{\nu_\ell}$ is:

$$\frac{d\Gamma_{\rm D^{+}}}{d\omega}(\omega) \;=\; \frac{{\rm G_F^2}}{48\pi^3} m^3_{\rm D^{+}} (m_{\rm B^0} + m_{\rm D^{+}})^2 (\omega^2-1)^{3/2} \mathcal{F}^2_{\rm D^{+}}(\omega) |V_{\rm cb}|^2, \qquad (2)$$

At zero recoil, $d\Gamma_{\rm D^+}/d\omega$ is much more suppressed due to helicity mismatch than in the case of $\overline{\rm B}^0 \to {\rm D}^{*+}\ell^-\overline{\nu_\ell}$. The strategy to extract $|V_{\rm cb}|$ is similar to that used for the decay $\overline{\rm B}^0 \to {\rm D}^{*+}\ell^-\overline{\nu_\ell}$ and the theoretical uncertainty in the determination of $|V_{\rm cb}|$ is of the same order [7].

In this letter an update of a previous measurement [4] of $\mathcal{F}_{\rm D^{*+}}(1)|V_{\rm cb}|$ from the decay $\overline{\rm B}^0 \to {\rm D}^{*+}\ell^-\overline{\nu_\ell}$ is presented and a first measurement of $\mathcal{F}_{\rm D^{+}}(1)|V_{\rm cb}|$ based on the study of $\overline{\rm B}^0 \to {\rm D}^{+}\ell^-\overline{\nu_\ell}$ decay is reported. The new analysis provides a new measurement of $|V_{\rm cb}|$ and it also allows a comparison of the form factors $\mathcal{F}_{\rm D^{*+}}(\omega)$ and $\mathcal{F}_{\rm D^{+}}(\omega)$ which are predicted to be identical at the infinitely heavy quark limit. The value of this ratio at zero recoil ($\omega = 1$) of the $\rm D^{(*)+}$ meson provides an important and direct test of the predictions of HQET. A value of $|V_{\rm cb}|$ is also extracted using almost model-independent constraints [7] on the slope and curvature of the hadronic form factors $\mathcal{F}_{\rm D^{*+}}(\omega)$ and $\mathcal{F}_{\rm D^{+}}(\omega)$.

2 The ALEPH detector

The ALEPH detector and its performance are described in detail in Ref. [8, 9]: only a brief description of the apparatus properties is given in this section. Charged particles are detected in the central part of the detector with three concentric devices, a precision vertex detector (VDET), a multi-wire drift chamber (ITC) and a large time projection chamber (TPC). Surrounding the beam pipe, the VDET consists of two concentric layers of double-sided silicon detectors, positioned at average radii of 6.5 cm and 11.3 cm, and covering respectively 85% and 69% of the solid angle. The intrinsic spatial resolution of the VDET is 12 μm for the $r\phi$ coordinate and between 11 μm and 22 μm for the z coordinate, depending on the polar angle of the charged particle. The ITC, at radii between 16 cm and 26 cm, provides up to 8 coordinates per track in the $r\phi$ view while the TPC measures up to 21 three-dimensional points per track at radii between 30 cm and 180 cm. The TPC also serves to identify charged particle species with up to 338 measurements of the specific ionization (dE/dx). The three detectors are immersed in an axial magnetic field of 1.5 T and together provide a transverse momentum resolution of $\sigma(1/p_T) = 0.6 \times 10^{-3}$ (GeV/c)$^{-1}$.

Electrons and photons are identified in the electromagnetic calorimeter (ECAL), a lead-proportional chamber sandwich segmented into 15 mrad $\times$ 15 mrad projective towers which are read out in three sections in depth. Muons are identified in the hadron calorimeter (HCAL), a 7 interaction length yoke interleaved with 23 layers of streamer tubes, together with two additional double layers of muon chambers.

The total visible energy in the detector is determined with an energy flow algorithm [9] which combines measurements from different detector components, to achieve a precision of $\sigma_E/\sqrt{E} = 0.60$ GeV$^{1/2}$.

3 Event selection

The analysis presented in this letter is based on approximately 3.9 million hadronic Z decays recorded with the ALEPH detector from 1991 to 1995 and selected as described in Ref. [10].

Exclusive semileptonic decays $\overline{\mathrm{B}}^0 \to \mathrm{D}^{*+}\ell^-\overline{\nu_\ell}$ and $\overline{\mathrm{B}}^0 \to \mathrm{D}^{+}\ell^-\overline{\nu_\ell}$ are selected in hadronic events where a lepton is associated with a D^{*+} or D^{+} respectively in the same hemisphere. Throughout this letter, "lepton" refers to either electron or muon, and charge conjugate reactions are implied.

The lepton identification is described in detail in Ref. [11]. Electrons are identified by their shower shape in the ECAL and when available, by the specific ionization information from the TPC. Muons are identified from their hit pattern in the HCAL and from the presence of at least one associated hit in the muon chambers. Electrons and muons are required to have momentum greater than 2 GeV/c and 3 GeV/c, respectively.

3.1 $\overline{\mathrm{B}}^0 \to \mathrm{D}^{*+}\ell^-\overline{\nu}_\ell$ event selection

D^{*+} candidates are reconstructed in the channel $\mathrm{D}^{*+} \to \mathrm{D}^0\pi^+$ and the D^0 candidates in the three decay modes: $\mathrm{D}^0 \to \mathrm{K}^-\pi^+$, $\mathrm{D}^0 \to \mathrm{K}^-\pi^+\pi^-\pi^+$ and $\mathrm{D}^0 \to \mathrm{K}^0_\mathrm{s}\pi^-\pi^+$. Candidate K^0_s are reconstructed in the channel $\mathrm{K}^0_\mathrm{s} \to \pi^-\pi^+$. The mass difference between the $\mathrm{D}^0\pi^+$ and the D^0 candidates is required to be within 2.1 MeV/c^2 (2.5 standard deviations) of 145.4 MeV/c^2. The event selection is similar to that described in Ref. [4].

Charged kaon candidates for which dE/dx information is available are required to have $|\chi_\mathrm{K}| < 2$, where χ_K is the number of standard deviations between the measured and the expected ionization for the kaon hypothesis. In the channels $\mathrm{D}^0 \to \mathrm{K}^-\pi^+\pi^-\pi^+$, kaon candidates with momenta less than 2 GeV/c are rejected. In the channel $\mathrm{K}^0_\mathrm{s} \to \pi^-\pi^+$, K^0_s candidates must have a momentum larger than 0.5 GeV/c, a decay length larger than 0.5 cm, and a reconstructed mass within 15 MeV/c^2 of the nominal K^0_s mass. Reconstructed D^0 candidates are required to have a vertex separated from the interaction point by more than twice the resolution on the D^0 reconstructed decay distance.

Reconstructed D^{*+} candidates are combined with an identified lepton from the same hemisphere and the angle between the D^{*+} and the lepton is required to be less than 45°. The $\mathrm{D}^{*+}\ell^-$ system is required to have an invariant mass less than 5.3 GeV/c^2. To ensure a good B meson vertex reconstruction, the lepton and at least two of the D^0 tracks are required to have one or more VDET hits. The χ^2 probabilities of the vertex fit for both D^0 and $\mathrm{D}^{*+}\ell^-$ vertices[1] must be larger than 1%. To ensure a precise measurement of the B meson direction and consequently a good ω reconstruction, the distance of the $\mathrm{D}^{*+}\ell^-$ vertex from the interaction point projected onto the $\mathrm{D}^{*+}\ell^-$ direction is required to be greater than 1 mm. The selection results in a sample of 1266 $\mathrm{D}^{*+}\ell^-$ candidates with a reconstructed D^0 mass within 2.5 standard deviations (σ = 10 MeV/c^2 for $\mathrm{D}^0 \to \mathrm{K}^-\pi^+$ and $\mathrm{D}^0 \to \mathrm{K}^0_\mathrm{s}\pi^-\pi^+$ and 8 MeV/c^2 for $\mathrm{D}^0 \to \mathrm{K}^-\pi^+\pi^-\pi^+$) of the D^0 nominal mass.

3.2 $\overline{\mathrm{B}}^0 \to \mathrm{D}^+\ell^-\overline{\nu}_\ell$ event selection

D^+ candidates are reconstructed in the channel $\mathrm{D}^+ \to \mathrm{K}^-\pi^+\pi^+$. Candidates kaon are selected as in the $\mathrm{D}^0 \to \mathrm{K}^-\pi^+\pi^-\pi^+$ channel, the momenta of the two pions are required to be greater than 1 GeV/c for the energetic pion and greater than 0.5 GeV/c for the other. Reflections from $\mathrm{D}^+_\mathrm{s} \to \mathrm{K}^-\mathrm{K}^+\pi^+$ are rejected if the $\mathrm{K}^-\mathrm{K}^+$ mass is within 6 MeV/c^2 of the ϕ meson mass or the $\mathrm{K}^-\pi^+$ mass is within 100 MeV/c^2 of the $\overline{\mathrm{K}}^{*0}$ mass and if the reconstructed $\mathrm{K}^+\mathrm{K}^-\pi^-$ mass is within 20 MeV/c^2 of the nominal D^+_s mass. Reconstructed D^+ candidates are required to have a vertex separated from the interaction point by more than five times the resolution of the D^+ decay distance.

Reconstructed D^+ candidates are combined with an identified lepton from the same hemisphere using the same selection criteria as in the $\mathrm{D}^{*+}\ell^-$ event selection. An additional requirement is placed on the distance between the D^+ vertex and

[1]The $\mathrm{D}^{*+}\ell^-$ vertex is determined from the lepton and the D^0 candidates.

the $D^+\ell^-$ vertex projected onto the D^+ direction which is required to be greater than -0.5 mm. The selection results in a sample of 1609 $D^+\ell^-$ candidates with a reconstructed D^+ mass within 2.5 standard deviations ($\sigma = 8$ MeV/c^2) of the D^+ nominal mass.

4 ω reconstruction

The ω reconstruction is performed on an event by event basis as described in Ref. [4]. It is computed from the B meson direction determined from the vector joining the $D^{(*)+}\ell^-$ vertex and the primary vertex, and the neutrino energy E_ν estimated from the missing energy in the hemisphere containing the $D^{(*)+}\ell^-$ candidate, as described in Ref. [12].

Fig. 1 shows the ω resolution averaged over all ω values for $\overline{B}^0 \to D^{*+}\ell^-\overline{\nu_\ell}$ and $\overline{B}^0 \to D^+\ell^-\overline{\nu_\ell}$ simulated Monte Carlo events. The average ω resolution is approximately 0.07 for both channels corresponding to 13% of the allowed kinematical range.

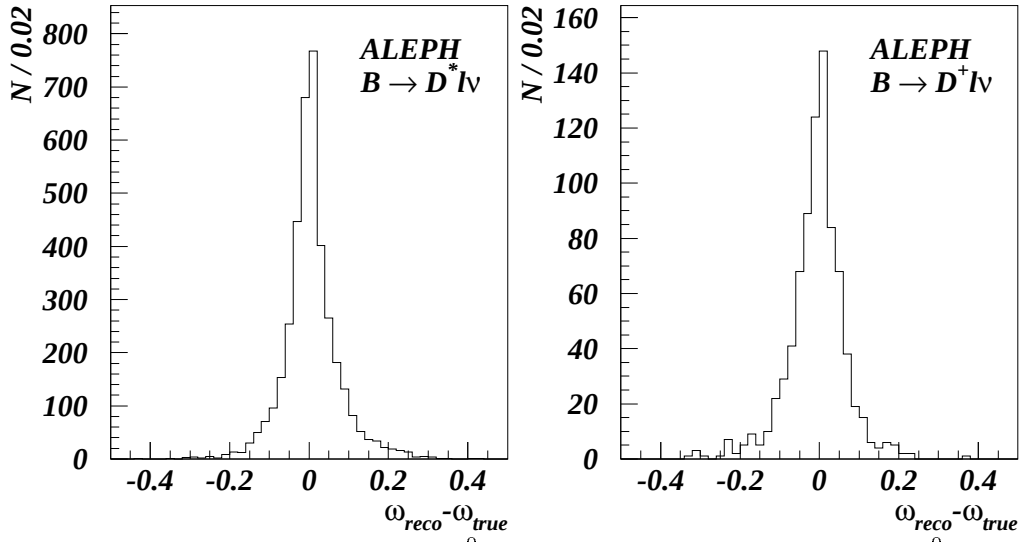

Figure 1: ω resolution for (a) $\overline{B}^0 \to D^{*+}\ell^-\overline{\nu_\ell}$ ($D^{*+} \to D^0\pi^+$), (b) $\overline{B}^0 \to D^+\ell^-\overline{\nu_\ell}$.

5 Sample composition and background rejection

5.1 Background sources

The two main classes of background sources that contribute to the $D^{(*)+}\ell^-$ are physics background processes where the $D^{(*)+}$ and the lepton are both real and combinatorial background events.

Physics background processes contributing to the $D^{*+}\ell^-$ and $D^+\ell^-$ samples and their measured or estimated branching ratios are listed in Table 1. Processes involving a D^{*+} meson in the final state contribute[2] to both $D^{*+}\ell^-$ and $D^+\ell^-$ samples while processes involving a D^+ meson contribute to the $D^+\ell^-$ sample only. Some of these processes have not been measured and are estimated from other measurements or by analogy with known decays. The branching ratios of $\overline{B}^0 \to D^{(*)+}\pi^0\ell^-\overline{\nu_\ell}$ and $\overline{B_s}^0 \to D^{(*)+}K^0\ell^-\overline{\nu_\ell}$ are estimated from measured values [13] of $Br(B^- \to D^{*+}\pi^-\ell^-\overline{\nu_\ell})$ and $Br(B^- \to D^+\pi^-\ell^-\overline{\nu_\ell})$, using isospin and flavour SU(3) symmetry. The branching ratios of $\overline{B}^0 \to D^{(*)+}\tau^-\overline{\nu_\tau}$ are estimated from the inclusive measurement $Br(b \to X\tau^-\nu_\tau)$ [14], assuming that three-fourths of $b \to X\tau^-\nu_\tau$ involve a D^{*+} meson and the other one-fourth involve a D^+ meson. The branching ratios of the inclusive processes $\overline{B} \to D^{*+}X_c$ and $\overline{B} \to D^+X_c$ are estimated from measured branching ratios of $\overline{B}^0 \to D^{*+}D_s^{(*)-}$ and $\overline{B}^0 \to D^+D_s^{(*)-}$ respectively, scaled by 1.2 ± 0.2 to allow for the possibility of n-body ($n \geq 3$) decays.

Table 1: Branching fraction of physics background processes used in this analysis.

Channels contributing to $D^{*+}\ell^-$ and $D^+\ell^-$	Branching fraction (%)	Channels contributing to $D^+\ell^-$	Branching fraction (%)
$B^- \to D^{*+}\pi^-\ell^-\overline{\nu_\ell}$	1.20 ± 0.26	$B^- \to D^+\pi^-\ell^-\overline{\nu_\ell}$	0.39 ± 0.25
$\overline{B}^0 \to D^{*+}\pi^0\ell^-\overline{\nu_\ell}$	0.60 ± 0.13	$\overline{B}^0 \to D^+\pi^0\ell^-\overline{\nu_\ell}$	0.20 ± 0.13
$\overline{B_s}^0 \to D^{*+}K^0\ell^-\overline{\nu_\ell}$	1.20 ± 0.26	$\overline{B_s}^0 \to D^+K^0\ell^-\overline{\nu_\ell}$	0.39 ± 0.25
$\overline{B}^0 \to D^{*+}\tau^-\overline{\nu_\tau}$	2.06 ± 0.41	$\overline{B}^0 \to D^+\tau^-\overline{\nu_\tau}$	0.69 ± 0.14
$\overline{B} \to D^{*+}X_c$	4.90 ± 1.60	$\overline{B} \to D^+X_c$	3.50 ± 2.00
		$\overline{B}^0 \to D^{*+}\ell^-\overline{\nu_\ell}$	5.14 ± 0.54

Combinatorial background events come from either a fake $D^{(*)+}$ in association with a real or a fake lepton, or a fake lepton in association with a real $D^{(*)+}$.

For the $D^{*+}\ell^-$ combinatorial background, fake D^{*+} arise from the combination of a fake D^0 with a random slow pion or from the combination of a real D^0 with a random slow pion. The first combination leads to a flat D^0 mass distribution under the D^0 mass peak in the $D^{*+}\ell^-$ sample. It is fitted with a second order polynomial function and its rate is estimated from the integral of the fitted function within the D^0 mass window. The rate of the second type of combination is estimated by assuming that the probability to associate a random soft pion to a genuine $D^0\ell^-$ pair, is the same as to associate a second soft pion to a reconstructed $D^{*+}\ell^-$ combination. This leads to a contribution of less than 1% of the signal at 95% confidence level. The fake lepton combinatorial background is estimated by applying a 1% (based on [11]) probability of hadron misidentification to D^{*+}-hadron combinations selected with the same criteria as $D^{*+}\ell^-$ combinations.

[2]The decay process $\overline{B}^0 \to D^{*+}\ell^-\overline{\nu_\ell}$ is the signal in the $D^{*+}\ell^-$ sample, and the main physics background component in the $D^+\ell^-$ sample. In Table 1 the $Br(\overline{B}^0 \to D^{*+}\ell^-\overline{\nu_\ell})$ value is the one measured from the $D^{*+}\ell^-$ sample (see section 6.1).

The $D^+\ell^-$ combinatorial background is estimated in a similar way. In addition, reflections from $D_s^+ \to K^-K^+\pi^+$ are reduced to less than 2% of the signal, as estimated from Monte-Carlo, with specific cuts as described in section 3. Reflections from $\Lambda_c^+ \to pK^-\pi^+$ and $D^{*+} \to D^0(\to K^-\pi^+X)\pi^+$ are negligible.

5.2 Background rejection

The expected composition of the $D^{*+}\ell^-$ and $D^+\ell^-$ samples after event selection requirements are presented in Table 2. The background level is clearly high especially in the $D^+\ell^-$ sample: the fraction of $D^{*+}\ell^-$ ($D^+\ell^-$) events originating from physics background processes is 27% (30%) and from combinatorial background is 16% (41%).

Table 2: The $D^{(*)+}\ell^-$ samples composition before (initial) and after (final) background rejection requirements.

	$D^{*+}\ell^-$ sample		$D^+\ell^-$ sample	
Sample composition	Initial	Final	Initial	Final
Yield	1266.0 ± 35.6	741.0 ± 27.2	1609.0 ± 40.1	465.0 ± 21.6
Physics background	342.3 ± 41.9	93.5 ± 11.2	485.8 ± 45.6	113.1 ± 8.9
Combi. background	204.0 ± 9.8	68.8 ± 4.6	654.2 ± 18.9	86.0 ± 4.7
Signal	720 ± 56	579 ± 30	469 ± 64	266 ± 24

To reduce the level of background in the two selected samples, three additional requirements are used. The contribution of the process $B^- \to D^{(*)+}\pi^-\ell^-\overline{\nu_\ell}$ in both samples is reduced by rejecting events where an additional charged particle is consistent with the B vertex. In particular, events with an additional charged track in a 45° cone around the $D^{(*)+}\ell^-$ direction, having the same charge as the lepton, momentum greater than 0.5 GeV/c, one or more VDET hits in $r\phi$ and z coordinates, and forming an invariant mass with the $D^{(*)+}\ell^-$ system lower than 5.3 GeV/c^2 are rejected if the charged track passes closer to the B vertex than to the interaction point and its impact parameter with respect to the B vertex is lower than 4σ. This requirement removes 77% of the $B^- \to D^{(*)+}\pi^-\ell^-\overline{\nu_\ell}$ background while keeping 96% of the signal. For the channels $D^+ \to K^-\pi^+\pi^+$ and $D^0 \to K^-\pi^+\pi^-\pi^+$, events with an additional track having a charge opposite to that of the lepton and satisfying the same criteria as described above but with the impact parameter calculated with respect to the D vertex instead of the B vertex, are rejected. This requirement removes 30% of the remaining combinatorial background while keeping 99 % of the signal.

To reject background $D^{(*)+}\ell^-$ events with additional particles originating from B decay, a missing mass variable $M^2_{\rm miss}$ is used as described in Ref. [4]. Candidates with $M^2_{\rm miss}$ greater than 1 GeV$^2/c^4$ are rejected. This requirement removes 49% of the $\overline{B}^0 \to D^{(*)+}\pi^0/K^0\ell^-\overline{\nu_\ell}$ while keeping 83% of the signal.

The contribution of background processes $\overline{B}^0 \to D^{*+}\ell^-\overline{\nu_\ell}$, $D^{*+} \to D^+\pi^0/\gamma$, (refered to hereafter $D^+\pi^0_*\ell^-$), to the $D^+\ell^-$ sample can be further reduced by rejecting

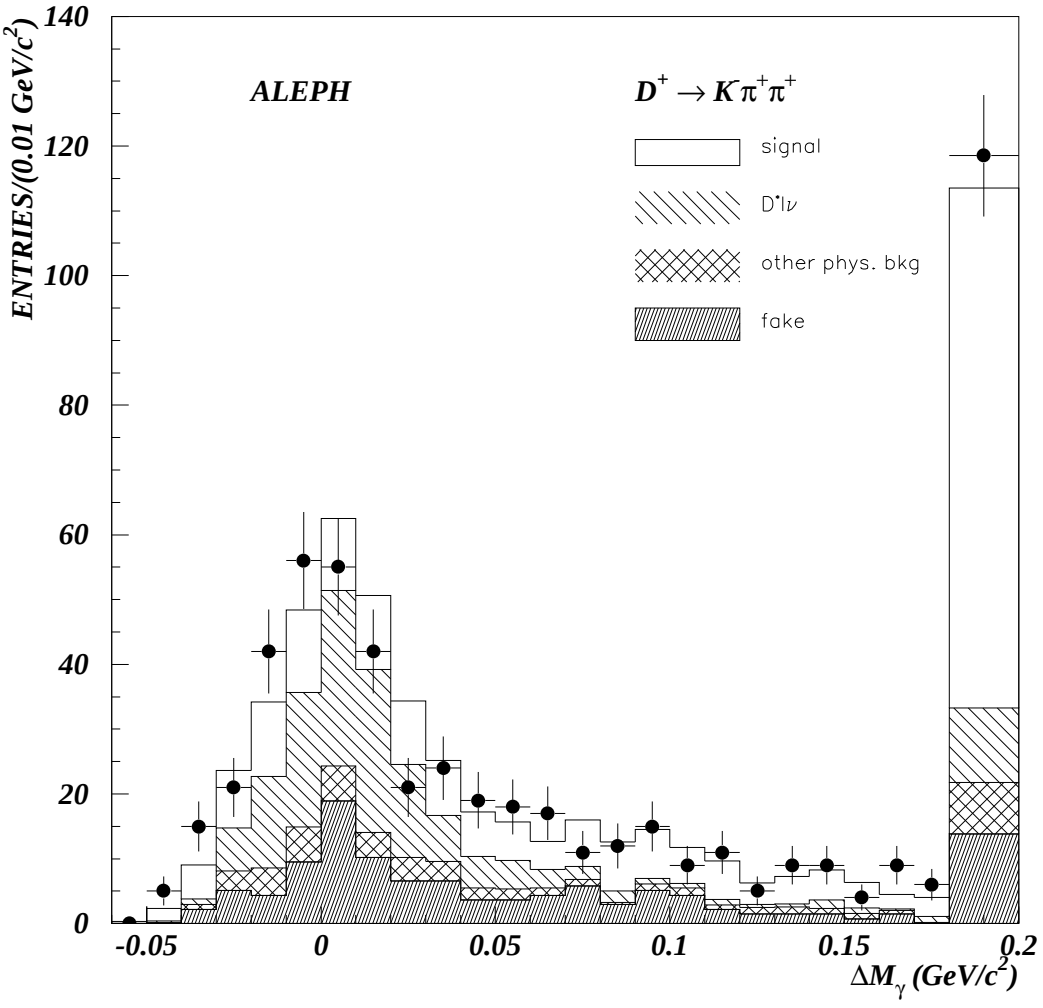

Figure 2: The reconstructed ΔM_γ for data (points), and backgrounds (histograms). If several photons are available, the one with ΔM_γ closest to zero is selected. The rightmost bin contains overflows and events with no photons. Its width is two times larger than the other bins.

$D^+\ell^-$ pairs correlated with a π^0 or a γ. Since $Br(D^{*+} \to D^+\gamma)$ is small compared to $Br(D^{*+} \to D^+\pi^0)$ [17], only π^0 particles are considered. Only one photon from π^0_* is searched for to avoid low reconstruction efficiency due to the soft π^0_* momentum in $D^{*+} \to D^+\pi^0$ decay. Photons with energy greater than 500 MeV are selected in a 45° cone around the D^+ direction. A mass difference variable is defined as $\Delta M_\gamma = M(D^+\gamma) - (M_{D^{*+}} + M_{D^+})/2$. Photons coming from $D^+\pi^0_*\ell^-$ are expected to cluster around zero in this variable. Events where $|\Delta M_\gamma| < 20$ MeV/c^2 are rejected. This requirement removes 54% of the $D^+\pi^0_*\ell^-$ background while keeping 83% of the $D^+\ell^-$ signal. Fig. 2 shows the reconstructed mass difference ΔM_γ for signal and background events.

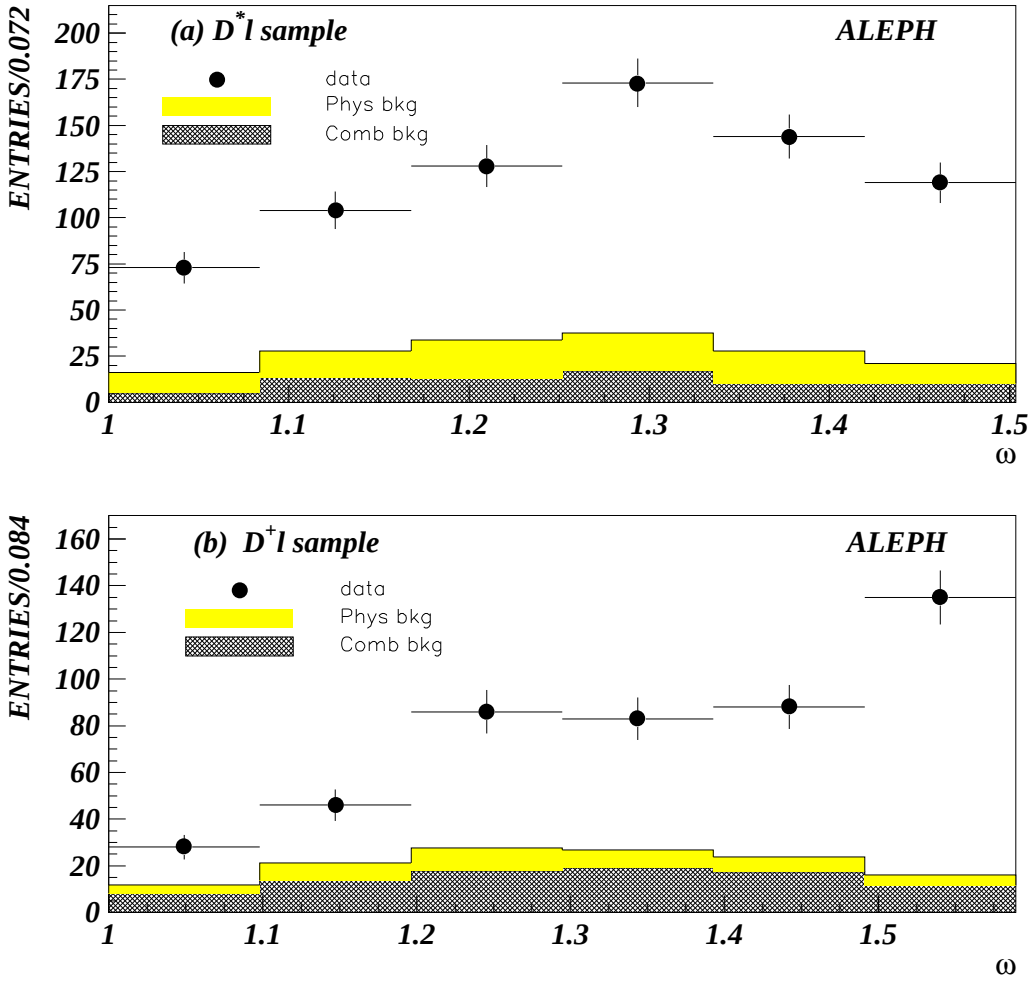

Figure 3: Reconstructed ω distributions for (a) $\overline{\mathrm{B}}^0 \to \mathrm{D}^{*+}\ell^-\overline{\nu_\ell}$ and (b) $\overline{\mathrm{B}}^0 \to \mathrm{D}^{+}\ell^-\overline{\nu_\ell}$ event candidates. The points are data, the black histograms are the combinatorial background contributions. The shaded histograms corresponds to the various physics backgrounds reconstructed from dedicated Monte Carlo. The $\mathrm{D}^+\pi^0_*\ell^-$ contribution in (b) is not shown, since it is to be fitted from data.

The expected composition of the $\mathrm{D}^{*+}\ell^-$ and $\mathrm{D}^+\ell^-$ samples after background rejection requirements are described in Table 2. The contribution of physics and combinatorial background events in the final $\mathrm{D}^{(*)+}\ell^-$ sample have been strongly reduced. The expected fraction of physics background $\mathrm{D}^{*+}\ell^-$ ($\mathrm{D}^+\ell^-$) events is 13% (24%). The expected fraction of combinatorial background $\mathrm{D}^{*+}\ell^-$ ($\mathrm{D}^+\ell^-$) events is 9% (18%). The purity of the final $\mathrm{D}^{*+}\ell^-$ ($\mathrm{D}^+\ell^-$) sample in $\overline{\mathrm{B}}^0 \to \mathrm{D}^{*+}\ell^-\overline{\nu_\ell}$ ($\overline{\mathrm{B}}^0 \to \mathrm{D}^{+}\ell^-\overline{\nu_\ell}$) is 78% (58%). The reconstructed ω distributions of the final $\mathrm{D}^{*+}\ell^-$ and $\mathrm{D}^+\ell^-$ samples are presented in Fig. 3 along with the main background contributions.

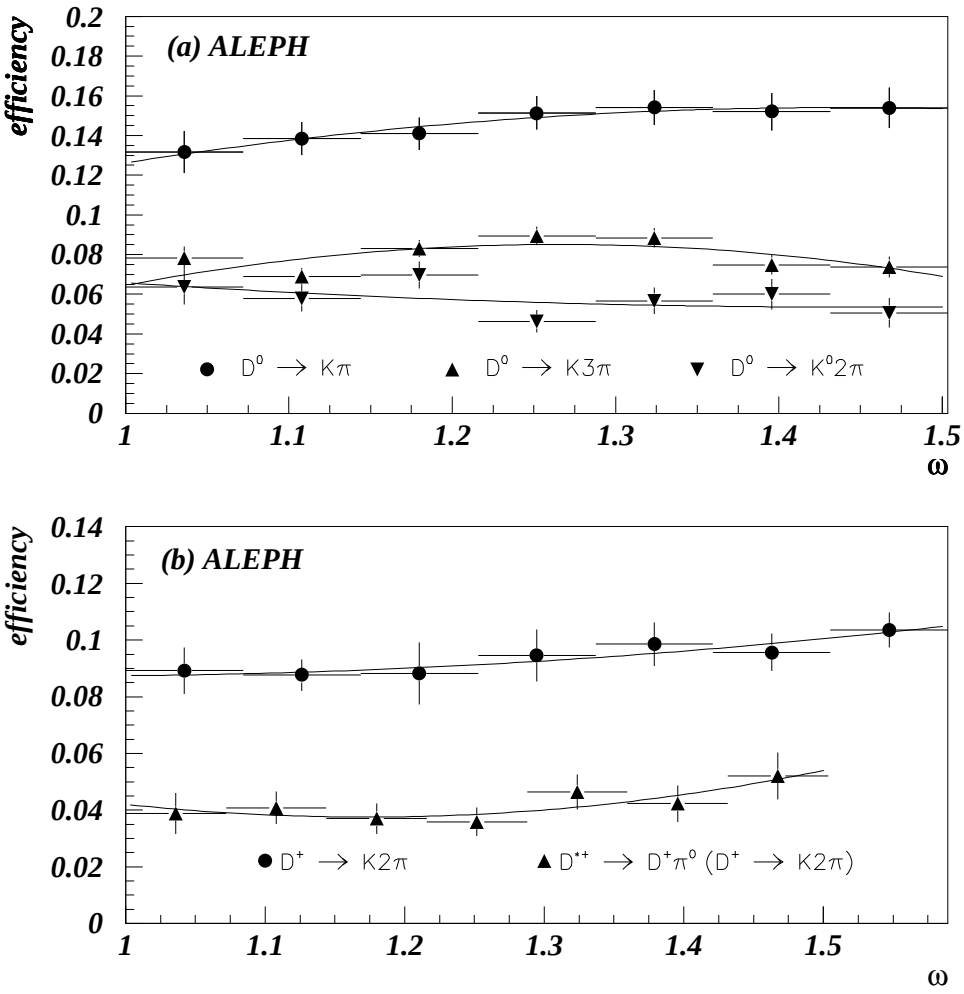

Figure 4: Reconstruction efficiency for (a) $\overline{\mathrm{B}}^0 \to \mathrm{D}^{*+}\ell^-\overline{\nu_\ell}$ decay and (b) $\overline{\mathrm{B}}^0 \to \mathrm{D}^+(\pi^0_*)\ell^-\overline{\nu_\ell}$ decay as a function of ω. The curves are the second order polynomial fits used to parameterise the efficiency in the fit.

The reconstruction efficiencies for $\overline{\mathrm{B}}^0 \to \mathrm{D}^{*+}\ell^-\overline{\nu_\ell}$ and $\overline{\mathrm{B}}^0 \to \mathrm{D}^+\ell^-\overline{\nu_\ell}$ decays are estimated from Monte Carlo simulation. Differences in efficiency of the VDET hits and vertices probability requirements between data and Monte Carlo are investigated in detail on inclusive D^{*+}, D^+, $\mathrm{D}^{*+}\ell^-$ and $\mathrm{D}^+\ell^-$ and corrections are applied to the simulation efficiencies [4]. The variation of the reconstruction efficiencies as a function of ω for all reconstructed decay channels are presented in Fig. 4.

Table 3: Branching fractions and lifetimes used. The quoted errors are used for the estimation of systematic uncertainties.

	Branching fractions (%)	Ref.
$\Gamma_{b\bar{b}}/\Gamma_{had}$	22.09 ± 0.21	[15]
$Br(b \to B^0)$	37.8 ± 2.2	[16]
$Br(b \to B_s^0)$	11.2 ± 1.9	[16]
$Br(D^{*+} \to D^0\pi^+)$	68.1 ± 1.3	[17]
$Br(D^{*+} \to D^+\pi^0)$	30.8 ± 0.8	[17]
$Br(D^{*+} \to D^+\gamma)$	$1.1^{+1.4}_{-0.7}$	[17]
$Br(D^0 \to K^-\pi^+)$	4.01 ± 0.14	[17]
$Br(D^0 \to K^-\pi^+\pi^-\pi^+)$	8.1 ± 0.5	[17]
$Br(D^0 \to K_s^0\pi^-\pi^+)$	2.6 ± 0.3	[17]
$Br(D^+ \to K^-\pi^+\pi^+)$	9.1 ± 0.6	[17]
	Lifetimes (ps)	Ref.
τ_{B^0}	1.564 ± 0.048	[18]
τ_{B^+}	1.617 ± 0.046	[18]
$\tau_{B_s^0}$	1.551 ± 0.106	[18]

6 Measurement of $\mathcal{F}_{D^{*+}}(1)|V_{cb}|$ and $\mathcal{F}_{D^+}(1)|V_{cb}|$

The method used to extract $\mathcal{F}_{D^{*+}}(1)|V_{cb}|$ and $\mathcal{F}_{D^+}(1)|V_{cb}|$ from the differential event rate $dN(D^{*+}\ell^-)/d\omega$ and $dN(D^+\ell^-)/d\omega$ is described in this section. The systematic error quoted for each result is described in the next section.

6.1 Measurement of $\mathcal{F}_{D^{*+}}(1)|V_{cb}|$

The combinatorial background contribution to $dN(D^{*+}\ell^-)/d\omega$ is measured from data in each bin of ω as described in section 5.1 while physics background contributions are taken from dedicated Monte Carlo simulation, with total number of events as given in Table 2.

The physics function which describes the $dN(D^{*+}\ell^-)/d\omega$ distribution of the final $\overline{B}^0 \to D^{*+}\ell^-\overline{\nu_\ell}$ sample after background subtraction is

$$\Phi(\omega) = 2\frac{N_{q\bar{q}}}{\epsilon_{q\bar{q}}}\frac{\Gamma_{b\bar{b}}}{\Gamma_{had}}Br(b \to B^0)Br(D^{*+} \to D^0\pi^+)Br(D^0 \to Kn\pi)\frac{\tau_{B^0}}{\hbar}\frac{d\Gamma_{D^{*+}}(\omega)}{d\omega}\epsilon(\omega) \ ,$$

where $Br(D^0 \to Kn\pi)$ is the branching ratio of the D^0 decay. Its value for the three decay channels is given in Table 3. The quantity $\epsilon_{q\bar{q}} = 97.4 \pm 0.24\%$ [10] is the hadronic event selection efficiency and $\epsilon(\omega)$ is the ω-dependent selection efficiency. The latter is parameterised for each D^0 decay channel by a second order polynomial. The differential decay width $d\Gamma_{D^{*+}}/d\omega$ is given in Eq. 1.

The unknowns in the physics function $\Phi(\omega)$ are $|V_{cb}|$ and $\mathcal{F}_{D^{*+}}(\omega)$. The dependence of $\mathcal{F}_{D^{*+}}(\omega)$ on ω is assumed to be linear:

$$\mathcal{F}_{D^{*+}}(\omega) = \mathcal{F}_{D^{*+}}(1)[1 - a^2_{D^{*+}}(1-\omega)]$$

A binned maximum likelihood fit is performed on the $dN(\mathrm{D}^{*+}\ell^-)/d\omega$ distribution. The fitting function is the convolution of the physics function $\Phi(\omega)$ and the ω-dependent resolution function. The fit yields the following 92.1% correlated results:

$$\begin{aligned} \mathcal{F}_{\mathrm{D}^{*+}}(1)|V_{\mathrm{cb}}| &= (30.6 \pm 1.8_{\mathrm{stat}} \pm 2.0_{\mathrm{syst}})\ 10^{-3}\ , \\ a^2_{\mathrm{D}^{*+}} &= 0.29 \pm 0.18_{\mathrm{stat}} \pm 0.12_{\mathrm{syst}}\ . \end{aligned}$$

Fig. 5a shows the result of the fit. The corresponding product $\mathcal{F}_{\mathrm{D}^{*+}}(\omega)|V_{\mathrm{cb}}|$ is shown in Fig. 5b. The value of $\mathcal{F}_{\mathrm{D}^{*+}}(\omega)|V_{\mathrm{cb}}|$ for specific values of the q^2 are useful for tests of the factorisation in hadronic decays; they are given in Table 4.

Table 4: Fitted values of $\mathcal{F}_{\mathrm{D}^+}(\omega)|V_{\mathrm{cb}}|$ and $\mathcal{F}_{\mathrm{D}^{*+}}(\omega)|V_{\mathrm{cb}}|$ for q^2 corresponding to the masses of some particles (note that the same q^2 corresponds to different ω depending on the decay). The values are also given for the maximum ω. The first uncertainties are statistical and the second are systematical.

	$\mathcal{F}_{\mathrm{D}^{*+}}(1)\lvert V_{\mathrm{cb}}\rvert(\times 10^{-3})$	$\mathcal{F}_{\mathrm{D}^+}(1)\lvert V_{\mathrm{cb}}\rvert(\times 10^{-3})$
$\omega = 1$	$30.6 \pm 1.8 \pm 2.0$	$28.6 \pm 6.7 \pm 6.9$
$\omega(m_{\mathrm{D}_s^+})$	$27.1 \pm 0.9 \pm 1.4$	$28.6 \pm 2.3 \pm 3.7$
$\omega(m_{a_1^+})$	$26.7 \pm 1.1 \pm 1.5$	$28.6 \pm 1.3 \pm 2.2$
$\omega(m_{\rho^+})$	$26.3 \pm 1.3 \pm 1.5$	$28.6 \pm 1.7 \pm 2.0$
$\omega(m_{\pi^+})$	$26.1 \pm 1.4 \pm 1.6$	$28.6 \pm 2.0 \pm 1.9$
$\omega^{max}_{\mathrm{D}^{*+}}$	$26.1 \pm 1.5 \pm 1.6$	$28.6 \pm 1.2 \pm 2.2$
$\omega^{max}_{\mathrm{D}^+}$	outside range	$28.6 \pm 2.1 \pm 1.9$

From the integrated physics function, the branching ratio of $\overline{\mathrm{B}}^0 \to \mathrm{D}^{*+}\ell^-\overline{\nu_\ell}$ is measured to be

$$\mathrm{Br}(\overline{\mathrm{B}}^0 \to \mathrm{D}^{*+}\ell^-\overline{\nu_\ell}) = (5.14 \pm 0.24_{\mathrm{stat}} \pm 0.48_{\mathrm{syst}})\%\ .$$

6.2 Measurement of $\mathcal{F}_{\mathrm{D}^+}(1)|V_{\mathrm{cb}}|$

All background contributions to $dN(\mathrm{D}^+\ell^-)/d\omega$ are estimated as described in the previous section except for the $\mathrm{D}^{*+}\ell^-$ component corresponding to the partially reconstructed $\mathrm{D}^+\pi^0_*\ell^-$ decay. The value of $\mathcal{F}_{\mathrm{D}^+}(1)|V_{\mathrm{cb}}|$ is extracted by fitting simultaneously the $dN(\mathrm{D}^+\ell^-)/d\omega$ and $dN(\mathrm{D}^{*+}\ell^-)/d\omega$ distributions so that the $\mathrm{D}^+\pi^0_*\ell^-$ background component in $dN(\mathrm{D}^+\ell^-)/d\omega$ is determined from data.

The physics function describing the $dN(\mathrm{D}^+\ell^-)/d\omega$ distribution after subtracting all backgrounds except the partially reconstructed $\mathrm{D}^+\pi^0_*\ell^-$ component is:

$$\begin{aligned} \Phi(\omega) &= 2\frac{N_{\mathrm{q\bar{q}}}}{\epsilon_{\mathrm{q\bar{q}}}}\frac{\Gamma_{\mathrm{b\bar{b}}}}{\Gamma_{\mathrm{had}}}\mathrm{Br}(\mathrm{b}\to \mathrm{B}^0)\mathrm{Br}(\mathrm{D}^+\to \mathrm{K}^-\pi^+\pi^+)\frac{\tau_{\mathrm{B}^0}}{\hbar} \\ &\times \left[\frac{d\Gamma_{\mathrm{D}^+}}{d\omega}(\omega)\epsilon_{\mathrm{D}^+}(\omega) + \mathrm{Br}(\mathrm{D}^{*+}\to \mathrm{D}^+\pi^0/\gamma)\frac{d\Gamma_{\mathrm{D}^{*+}}}{d\omega}(\omega)\epsilon_{\mathrm{D}^{*+}}(\omega)\right]\ . \end{aligned}$$

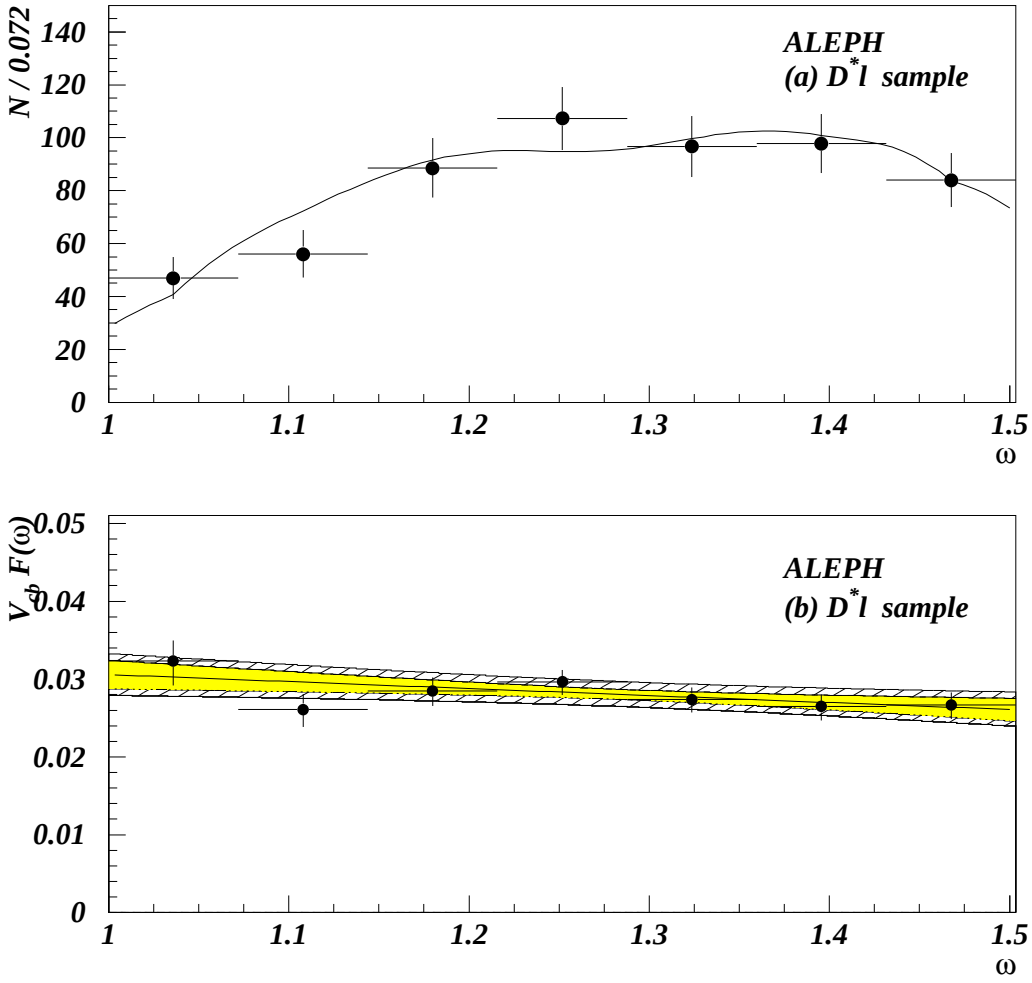

Figure 5: (a) The differential rate $dN(\mathrm{D}^{*+}\ell^-)/d\omega$ of $\overline{\mathrm{B}}^0 \to \mathrm{D}^{*+}\ell^-\overline{\nu_\ell}$ candidates after all cuts and background subtraction. The points are data with statistical error bars, and the curve is the result of the fit. (b) $\mathcal{F}_{\mathrm{D}^{*+}}(\omega)|V_{\mathrm{cb}}|$ as a function of ω, the shaded band and the hatched bands indicating the statistical and systematic uncertainties, respectively. The points are data after removal of all known terms of the physics function and correcting for resolution effects.

The ω-dependent selection efficiencies $\epsilon_{\mathrm{D}^+}(\omega)$ for the $\overline{\mathrm{B}}^0 \to \mathrm{D}^+\ell^-\overline{\nu_\ell}$ signal and $\epsilon_{\mathrm{D}^{*+}}(\omega)$ for the $\overline{\mathrm{B}}^0 \to \mathrm{D}^{*+}\ell^-\overline{\nu_\ell}$ background are both parameterised by second order polynomials. The differential decay widths $d\Gamma_{\mathrm{D}^{*+}}/d\omega$ and $d\Gamma_{\mathrm{D}^+}/d\omega$ are given in Eqs. 1 and 2, respectively. The form factor $\mathcal{F}_{\mathrm{D}^+}(\omega)$ in $d\Gamma_{\mathrm{D}^+}/d\omega$ is assumed to have a linear dependence on ω, as for $\mathcal{F}_{\mathrm{D}^{*+}}(\omega)$ in $d\Gamma_{\mathrm{D}^{*+}}/d\omega$:

$$\mathcal{F}_{\mathrm{D}^+}(\omega) = \mathcal{F}_{\mathrm{D}^+}(1)[1 - a^2_{\mathrm{D}^+}(1-\omega)] \; .$$

A binned maximum likelihood fit is simultaneously performed on the $dN(\mathrm{D}^+\ell^-)/d\omega$

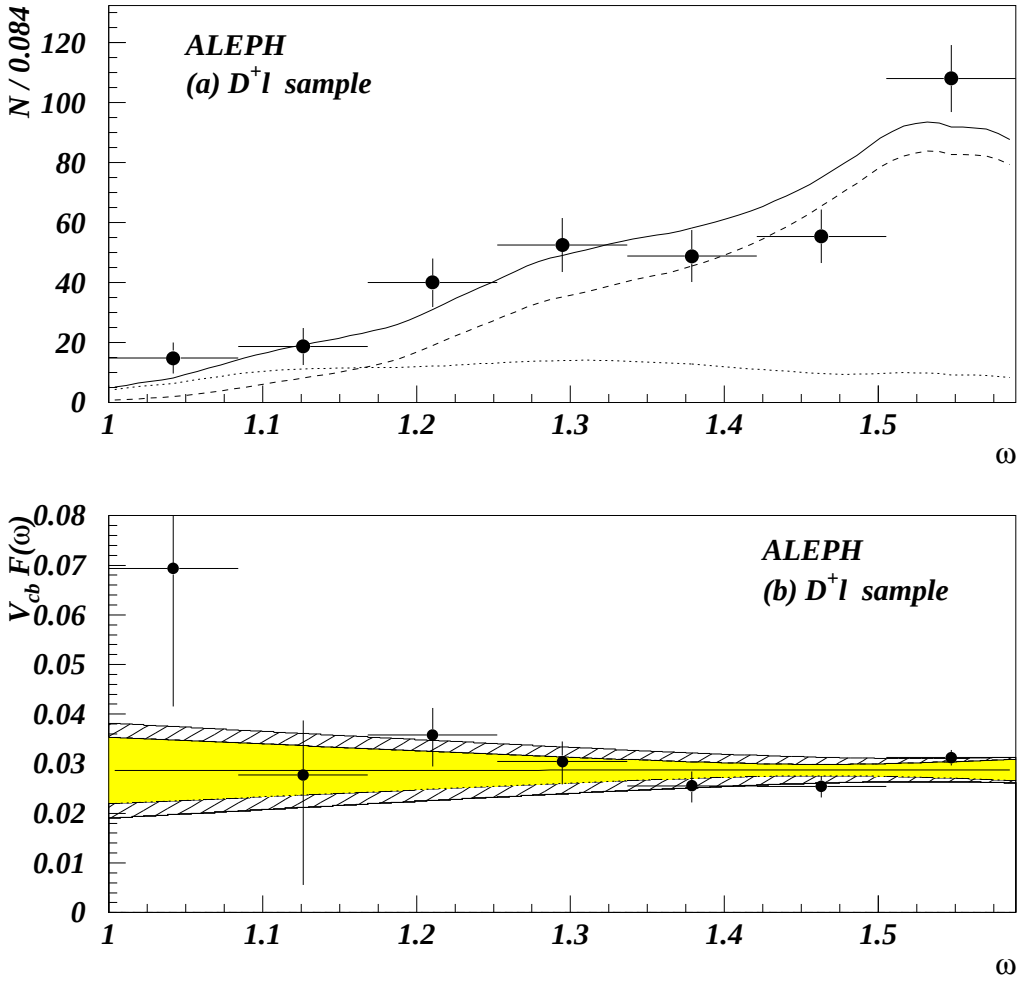

Figure 6: (a) The differential event rate $dN(\mathrm{D}^{+}\ell^{-})/d\omega$ of $\overline{\mathrm{B}}^{0}\to \mathrm{D}^{+}\ell^{-}\overline{\nu_\ell}$ candidates after all cuts and background subtraction. The points are data with statistical error bars, the dotted curve is the $\mathrm{D}^{0}\pi^{+}_{*}\ell^{-}$ background ω-distribution, the dashed curve is the $\overline{\mathrm{B}}^{0}\to \mathrm{D}^{+}\ell^{-}\overline{\nu_\ell}$ ω-distribution and the solid curve the sum of the two. (b) $\mathcal{F}_{\mathrm{D}^{+}}(\omega)|V_{\mathrm{cb}}|$ as a function of ω (see caption of Fig. 5 for details).

and $dN(\mathrm{D}^{*+}\ell^{-})/d\omega$ distributions. The signal and background components of the $dN(\mathrm{D}^{+}\ell^{-})/d\omega$ distribution are convolved with different ω-resolution functions. The ω-resolution function for background $\mathrm{D}^{+}\pi^{0}_{*}\ell^{-}$ events is worsened due to the missing π^{0}. The four free parameters in the fit are $\mathcal{F}_{\mathrm{D}^{+}}(1)|V_{\mathrm{cb}}|$, $a^{2}_{\mathrm{D}^{+}}$, $\mathcal{F}_{\mathrm{D}^{*+}}(1)|V_{\mathrm{cb}}|$, and $a^{2}_{\mathrm{D}^{*+}}$. The fit yields the following 98.6% correlated results:

$$\begin{aligned}\mathcal{F}_{\mathrm{D}^{+}}(1)|V_{\mathrm{cb}}| &= (28.8 \pm 6.7_{\mathrm{stat}} \pm 6.9_{\mathrm{syst}})\ 10^{-3}\ ,\\ a^{2}_{\mathrm{D}^{+}} &= 0.00 \pm 0.49_{\mathrm{stat}} \pm 0.38_{\mathrm{syst}}\ .\end{aligned}$$

The statistical uncertainties include by construction the uncertainty on the $\mathrm{D}^{*+}\ell^-$ contribution. The values of $\mathcal{F}_{\mathrm{D}^{*+}}(1)|V_{\mathrm{cb}}|$ and $a^2_{\mathrm{D}^{*+}}$ obtained from the simultaneous fit are similar to those obtained from a fit of $dN(\mathrm{D}^{*+}\ell^-)/d\omega$ distribution alone. Fig. 6a shows the result of the fit. The corresponding product $\mathcal{F}_{\mathrm{D}^+}(\omega)|V_{\mathrm{cb}}|$ is shown in Fig. 6b. The value of $\mathcal{F}_{\mathrm{D}^+}(\omega)|V_{\mathrm{cb}}|$ for specific values of the q^2 are also given in Table 4.

From the integrated physics function $\Phi_{\mathrm{D}^+}(\omega)$, the branching ratio of $\overline{\mathrm{B}}^0 \to \mathrm{D}^+\ell^-\overline{\nu_\ell}$ is measured to be

$$\mathrm{Br}(\overline{\mathrm{B}}^0 \to \mathrm{D}^+\ell^-\overline{\nu_\ell}) = (2.41 \pm 0.22_{\mathrm{stat}} \pm 0.44_{\mathrm{syst}})\% \ .$$

6.3 Measurement of $\mathcal{F}_{\mathrm{D}^+}(1)/\mathcal{F}_{\mathrm{D}^{*+}}(1)$ and $|V_{\mathrm{cb}}|$

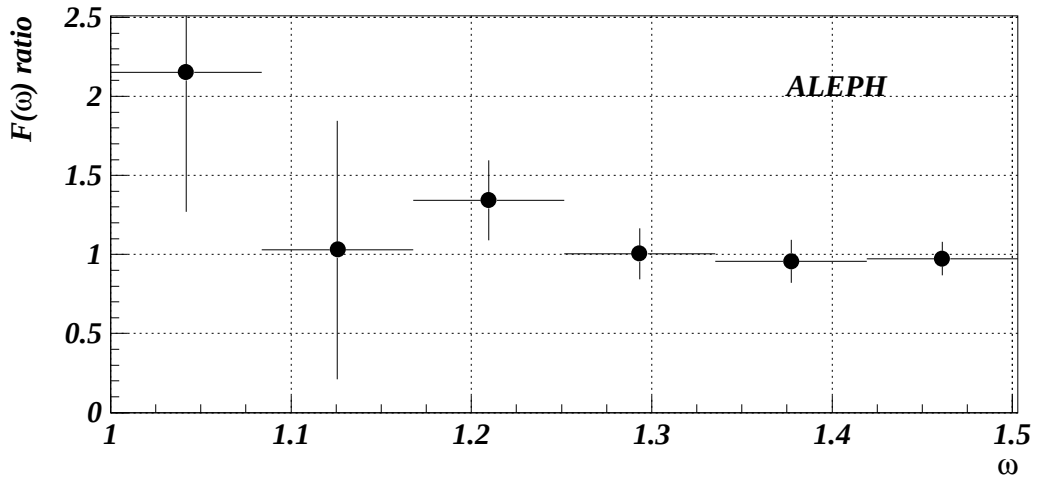

Figure 7: The ratio of $\mathcal{F}_{\mathrm{D}^+}(\omega)$ and $\mathcal{F}_{\mathrm{D}^{*+}}(\omega)$.

Fig. 7 shows that the ratio of $\mathcal{F}_{\mathrm{D}^+}(\omega)|V_{\mathrm{cb}}|$ and $\mathcal{F}_{\mathrm{D}^{*+}}(\omega)|V_{\mathrm{cb}}|$ distributions is consistent with unity over the whole common range of ω. At $\omega = 1$ this ratio is measured from the results of the previous fits to be

$$\frac{\mathcal{F}_{\mathrm{D}^+}(1)}{\mathcal{F}_{\mathrm{D}^{*+}}(1)} = 0.94 \pm 0.23_{\mathrm{stat}} \pm 0.23_{\mathrm{syst}} \ ,$$

which is in agreement with the theoretical prediction [7]:

$$\frac{\mathcal{F}^{\mathrm{th}}_{\mathrm{D}^+}(1)}{\mathcal{F}^{\mathrm{th}}_{\mathrm{D}^{*+}}(1)} = 1.08 \pm 0.06_{\mathrm{th}} \ ,$$

The same quantity can be calculated with better accuracy at $\omega^{max}_{\mathrm{D}^{*+}}$ the maximum value of ω for the $\overline{\mathrm{B}}^0 \to \mathrm{D}^{*+}\ell^-\overline{\nu_\ell}$ decay

$$\frac{\mathcal{F}_{\mathrm{D}^+}(\omega^{max}_{\mathrm{D}^{*+}})}{\mathcal{F}_{\mathrm{D}^{*+}}(\omega^{max}_{\mathrm{D}^{*+}})} = 1.10 \pm 0.08_{\mathrm{stat}} \pm 0.11_{\mathrm{syst}},$$

which is consistent with 1.

The independence of $\frac{\mathcal{F}_{\mathrm{D}^+}(\omega)}{\mathcal{F}_{\mathrm{D}^{*+}}(\omega)}$ on ω over the whole range of ω can also be quantified by comparing the fitted slopes of the two channels:

$$a^2_{\mathrm{D}^+} - a^2_{\mathrm{D}^{*+}} = -0.30 \pm 0.55_{\mathrm{stat}} \ ,$$

in agreement with the theoretical value [7]:

$$(a^2_{\mathrm{D}^+} - a^2_{\mathrm{D}^{*+}})_{\mathrm{th}} \simeq 0.08 \ .$$

These tests are the first tests of the prediction of HQET that the decays $\overline{\mathrm{B}}^0 \to \mathrm{D}^{*+}\ell^-\overline{\nu_\ell}$ and $\overline{\mathrm{B}}^0 \to \mathrm{D}^+\ell^-\overline{\nu_\ell}$ can be described by the same hadronic form factor. This prediction can be exploited to extract $|V_{\mathrm{cb}}|$ from the two decays, by using the Isgur-Wise function $\mathcal{F}_0(\omega)$ itself. A second-order parameterisation

$$\mathcal{F}_0(\omega) = 1 - a^2_0(\omega - 1) + c_0(\omega - 1)^2$$

is chosen and a theoretical constraint [7] $c_0 \simeq 0.72a^2_0 - 0.09$ is used. The form factors $\mathcal{F}_{\mathrm{D}^{*+}}(\omega)$ and $\mathcal{F}_{\mathrm{D}^+}(\omega)$ are parameterised similarly, with slopes and curvatures related to the one of $\mathcal{F}_0(\omega)$ by the relations [7] $a^2_{\mathrm{D}^{*+}} = a^2_0 - 0.06$, $a^2_{\mathrm{D}^+} = a^2_0 + 0.02$, $c_{\mathrm{D}^{*+}} = c_0 - 0.06 - 0.06a^2_0$, $c_{\mathrm{D}^+} = c_0 + 0.01 + 0.02a^2_0$. These relations give the possibility to translate the constraint between a^2_0 and c_0 into constraints between $a^2_{\mathrm{D}^{(*)+}}$ and $c_{\mathrm{D}^{(*)+}}$, yielding the following results:

$$\begin{aligned}
\mathcal{F}_{\mathrm{D}^{*+}}(1)|V_{\mathrm{cb}}| &= (30.6 \pm 2.1_{\mathrm{stat}} \pm 2.0_{\mathrm{syst}})\ 10^{-3} \ , \\
a^2_{\mathrm{D}^{*+}} &= 0.34 \pm 0.27_{\mathrm{stat}} \pm 0.12_{\mathrm{syst}} \ , \\
\mathcal{F}_{\mathrm{D}^+}(1)|V_{\mathrm{cb}}| &= (32.2 \pm 9.8_{\mathrm{stat}} \pm 8.6_{\mathrm{syst}})\ 10^{-3} \ , \\
a^2_{\mathrm{D}^+} &= 0.29 \pm 0.91_{\mathrm{stat}} \pm 0.5_{\mathrm{syst}} \ .
\end{aligned}$$

The increase of the uncertainty is the price to pay for a less arbitrary parameterisation of the form factors.

The measurement of $|V_{\mathrm{cb}}|$ is done by fitting directly the Isgur-Wise function with the parameterisation given above and taking the normalisations at $\omega = 1$ to be $\mathcal{F}^{\mathrm{th}}_{\mathrm{D}^{*+}}(1) = 0.91 \pm 0.03_{\mathrm{th}}$ and $\frac{\mathcal{F}^{\mathrm{th}}_{\mathrm{D}^+}(1)}{\mathcal{F}^{\mathrm{th}}_{\mathrm{D}^{*+}}(1)} = 1.08 \pm 0.06_{\mathrm{th}}$ [20]. The fitted values of the two remaining free parameters, which are 95.0% correlated, are:

$$\begin{aligned}
|V_{\mathrm{cb}}| &= (33.4 \pm 2.0_{\mathrm{stat}} \pm 2.3_{\mathrm{syst}} \pm 1.3_{\mathrm{th}})\ 10^{-3} \ , \\
a^2_0 &= 0.35 \pm 0.22_{\mathrm{stat}} \pm 0.14_{\mathrm{syst}} \pm 0.13_{\mathrm{th}} \ .
\end{aligned}$$

Table 5: Systematic uncertainties. All contributions are given in percent with respect to the measured value except for $a^2_{\mathrm{D}^+}$ and $a^2_{\mathrm{D}^{*+}}$, where absolute uncertainties are quoted.

Source	$\mathcal{F}_{\mathrm{D}^{*+}}(1)\lvert V_{\mathrm{cb}}\rvert$	$a^2_{\mathrm{D}^{*+}}$	$\mathrm{Br}_{\mathrm{D}^{*+}}$	$\mathcal{F}_{\mathrm{D}^+}(1)\lvert V_{\mathrm{cb}}\rvert$	$a^2_{\mathrm{D}^+}$	$\mathrm{Br}_{\mathrm{D}^+}$	$\frac{\mathcal{F}_{\mathrm{D}^{*+}}(1)}{\mathcal{F}_{\mathrm{D}^+}(1)}$
Branching ratios							
$\mathrm{Br}(\mathrm{D}\to \mathrm{K}n\pi)$	2.4	-	4.7	10.0	0.13	9.5	11.1
$\mathrm{Br}(\mathrm{D}^{*+}\to \mathrm{D}^0\pi^+)$	1.4	-	2.8	4.6	0.08	2.1	5.9
$\Gamma_{\mathrm{b\overline{b}}}/\Gamma_{had}$	0.6	-	1.1	0.7	-	1.0	-
$\mathrm{Br}(\mathrm{b}\to \mathrm{B}^0)$	2.4	-	4.6	2.5	-	5.6	-
Subtotal	3.7	-	7.2	11.3	0.15	11.2	12.6
Background							
$\mathrm{B}^-\to \mathrm{D}^*X\ell^-\overline{\nu_\ell}$	2.1	0.02	2.8	3.6	0.07	1.5	5.7
$\mathrm{B}^-\to \mathrm{D}^+X\ell^-\overline{\nu_\ell}$	-	-	-	11.7	0.22	4.9	11.4
$\overline{\mathrm{B}}\to \mathrm{D}^{(*)+}\mathrm{X_c}$	0.1	0.01	0.5	1.7	0.03	1.1	1.7
$\overline{\mathrm{B}}^0\to \mathrm{D}^{(*)+}\tau^-\overline{\nu_\tau}$	0.2	-	0.4	1.8	0.04	0.5	1.6
Fake $\mathrm{D}^{(*)}$	0.8	-	1.6	2.2	0.01	2.2	2.9
Fake lepton	0.7	-	0.4	1.1	0.02	0.5	1.0
Subtotal	2.4	0.03	3.2	12.7	0.23	5.6	13.3
Simulation							
Fragmentation	1.7	0.02	2.3	3.6	0.03	4.7	2.1
ℓ efficiency	1.5	-	3.0	3.0	0.02	3.0	0.3
Vertex efficiency	1.5	-	2.9	11.2	0.13	10.5	11.2
Photon efficiency	-	-	-	6.0	0.04	6.0	6.0
Efficiency shape	0.6	0.02	0.3	4.5	0.10	0.4	5.1
MC statistics	1.7	0.05	1.6	8.1	0.17	2.6	8.6
ω resolution	3.0	0.10	-	3.0	0.10	-	3.0
Subtotal	4.4	0.12	5.0	16.7	0.26	13.6	16.6
B^0 **lifetime**	2.1	-	1.2	2.6	0.01	1.1	0.3
Total	6.6	0.12	9.4	23.8	0.38	18.5	24.7

7 Systematic uncertainties

The various sources of systematic uncertainties are summarized in Table 5. They are described in more detail below. Since $\mathcal{F}(1)|V_{\mathrm{cb}}|$ is proportional to the square root of the branching fraction of the B decay, it will be twice less sensitive than the branching fractions to quantities like other branching fractions and efficiencies, provided the slope a^2 is unaffected. This is generally true for the $\mathrm{D}^{*+}\ell^-$ channel, where the signal and the background have similar shapes. For the $\mathrm{D}^+\ell^-$ channel however, the signal vanishes rapidly at low ω, while the background is roughly constant. Any systematic affecting the background level will affect both the normalisation and the slope, with a comparatively higher impact on $\mathcal{F}(1)|V_{\mathrm{cb}}|$ than for the $\mathrm{D}^{*+}\ell^-$ channel. Correlations between the $\mathrm{D}^{*+}\ell^-$ and the $\mathrm{D}^+\ell^-$ measurements are taken into account in the determination of all uncertainties. The total systematic uncertainties on $\mathcal{F}_{\mathrm{D}^{*+}}(1)|V_{\mathrm{cb}}|(\mathcal{F}_{\mathrm{D}^+}(1)|V_{\mathrm{cb}}|)$ and $a^2_{\mathrm{D}^{*+}}(a^2_{\mathrm{D}^+})$ are 76%(96%) correlated.

Branching fractions: The systematic uncertainties related to the fraction of hadronic Z decays to $b\overline{b}$ pairs and the D^{*+}, D^0 and D^+ branching fractions are estimated by the effect of their variation within the quoted uncertainties in Table 3. Correlations in the measured D^0 branching fractions are taken into account. The branching ratios $Br(D^{*+} \to D^0\pi^+)$ and $Br(D^{*+} \to D^+\pi^0/\gamma)$ are also taken to be fully anti-correlated.

Backgrounds: The contribution of each physics background is varied within uncertainties given in Table 1, taking into account their possible correlation. The fraction of resonant decays in the Monte Carlo simulation is varied between 0 and 100% (with a central value of 55% [13]) to account for the lack of knowledge of the non-resonant part.

The use of a first order polynomial instead of a second order one to describe the fake D background component in the D mass spectrum fit changes the background estimate slightly. The contribution of fake D^{*+} events in the $D^{*+}\ell^-$ sample and of the reflection from $D_s^+ \to K^-K^+\pi^+$ in the $D^+\ell^-$ sample are varied by 100 % of their estimated contribution given in 5.1. The uncertainty on the fake lepton misidentification probability (electron or muon) is estimated to be 20%, based on [11].

Simulation: The mean B hadron momentum has been measured by ALEPH to be : $x_B = 0.714 \pm 0.012$ [19]. The quoted uncertainty corresponds to the variation of the efficiency when x_B is varied within errors. The uncertainty on the lepton efficiency is taken to be 3%, based on [11].

The data *vs* Monte Carlo efficiency ratio of the VDET hits and vertex probability requirements evaluated in 5.2 are varied within errors.

Photon reconstruction affects the selected $D^+\ell^-$ sample in two ways. The efficiency for associating the D^+ with a random photon affects directly the $D^+\ell^-$ efficiency. This effect is checked by comparing in data and Monte Carlo the probability to associate a random photon to $D^0\pi_*^+\ell^-$ events, where no photon is expected. The photon reconstruction efficiency directly affects the level of remaining $D^+\pi_*^0\ell^-$ events. This effect is checked by comparing the number of $D^+\pi_*^0\ell^-$ events passing and failing the photon rejection cut on data and Monte Carlo. The quoted uncertainty corresponds to the statistical error of these two checks.

The uncertainty related to the ω resolution is taken to be half of the change in parameters when the fit is performed with a perfect resolution. Degrading the ω resolution by arbitrarily shifting the missing energy or smearing the vertices by one event-by-event uncertainty, or by not using the soft pion in the $D^{*+}\ell^-$ channel does not change the result by more than this uncertainty.

The uncertainty related to the dependence of the efficiency with ω corresponds to the change if the fit is performed with a linear instead of quadratic parameterisation of the efficiency *vs* ω.

B lifetimes: A change in B^0 lifetime affects $\mathcal{F}(1)|V_{cb}|$ in two ways. An increase in the lifetime directly decreases the partial width corresponding to a fixed branching ratio. However the branching ratio also decreases because the requirement on the decay length above 1 mm favour long lifetime events. A change in the B^+ and B_s^0 lifetimes within errors also affects the proportion of physics background but this has a negligible effect on the final results.

8 Conclusion

The differential decay rates $d\Gamma/d\omega$ for the decays $\overline{\mathrm{B}}^0 \to \mathrm{D}^{*+}\ell^-\overline{\nu_\ell}$ and $\overline{\mathrm{B}}^0 \to \mathrm{D}^{+}\ell^-\overline{\nu_\ell}$ are measured. Using linear ω dependence for the hadronic form factors $\mathcal{F}_{\mathrm{D}^{*+}}(\omega)$ and $\mathcal{F}_{\mathrm{D}^{+}}(\omega)$, the values of $\mathcal{F}_{\mathrm{D}^{*+}}(1)|V_{\mathrm{cb}}|$ and $\mathcal{F}_{\mathrm{D}^{+}}(1)|V_{\mathrm{cb}}|$ and of the slopes $a^2_{\mathrm{D}^{*+}}$ and $a^2_{\mathrm{D}^{+}}$ are:

$$\begin{aligned} \mathcal{F}_{\mathrm{D}^{*+}}(1)|V_{\mathrm{cb}}| &= (30.6 \pm 1.8_{\mathrm{stat}} \pm 2.0_{\mathrm{syst}})\ 10^{-3}\ , \\ a^2_{\mathrm{D}^{*+}} &= 0.29 \pm 0.18_{\mathrm{stat}} \pm 0.12_{\mathrm{syst}}\ , \end{aligned}$$

and

$$\begin{aligned} \mathcal{F}_{\mathrm{D}^{+}}(1)|V_{\mathrm{cb}}| &= (28.8 \pm 6.7_{\mathrm{stat}} \pm 6.9_{\mathrm{syst}})\ 10^{-3}\ , \\ a^2_{\mathrm{D}^{+}} &= 0.00 \pm 0.49_{\mathrm{stat}} \pm 0.38_{\mathrm{syst}}\ . \end{aligned}$$

The values of $\mathcal{F}_{\mathrm{D}^{*+}}(1)|V_{\mathrm{cb}}|$ and $a^2_{\mathrm{D}^{*+}}$ are in agreement with the previous ALEPH measurement [4] with greater accuracy.

The ratio of the form factors $\mathcal{F}_{\mathrm{D}^{*+}}(\omega)$ and $\mathcal{F}_{\mathrm{D}^{+}}(\omega)$ at $\omega = 1$ and $\omega = \omega^{max}_{\mathrm{D}^{*+}}$ and the difference of their slopes are measured to be

$$\begin{aligned} \frac{\mathcal{F}_{\mathrm{D}^{+}}(1)}{\mathcal{F}_{\mathrm{D}^{*+}}(1)} &= 0.94 \pm 0.23_{\mathrm{stat}} \pm 0.23_{\mathrm{syst}}\ , \\ \frac{\mathcal{F}_{\mathrm{D}^{+}}(\omega^{max}_{\mathrm{D}^{*+}})}{\mathcal{F}_{\mathrm{D}^{*+}}(\omega^{max}_{\mathrm{D}^{*+}})} &= 1.10 \pm 0.08_{\mathrm{stat}} \pm 0.11_{\mathrm{syst}}, \\ a^2_{\mathrm{D}^{+}} - a^2_{\mathrm{D}^{*+}} &= -0.30 \pm 0.55_{\mathrm{stat}} \pm 0.31_{\mathrm{syst}}\ . \end{aligned}$$

These measured values are in agreement with theoretical predictions from HQET. They represent the first tests of HQET prediction of the universality of the Isgur-Wise function.

Using theoretical constraints on the slope and curvature of the hadronic form factors and their calculated values at $\omega = 1$, $|V_{\mathrm{cb}}|$ is measured to be

$$|V_{\mathrm{cb}}| = (33.4 \pm 2.0_{\mathrm{stat}} \pm 2.3_{\mathrm{syst}} \pm 1.4_{\mathrm{th}})\ 10^{-3}\ .$$

The slope of the Isgur-Wise function is

$$a^2_0 = 0.35 \pm 0.22_{\mathrm{stat}} \pm 0.14_{\mathrm{syst}} \pm 0.13_{\mathrm{th}}\ .$$

This measured value is within the expected theoretical bounds [7].

The integrated spectra of the two semileptonic B^0 decay channels yield the following branching fractions:

$$\begin{aligned} \mathrm{Br}(\overline{\mathrm{B}}^0 \to \mathrm{D}^{*+}\ell^-\overline{\nu_\ell}) &= (5.14 \pm 0.24_{\mathrm{stat}} \pm 0.48_{\mathrm{syst}})\%\ , \\ \mathrm{Br}(\overline{\mathrm{B}}^0 \to \mathrm{D}^{+}\ell^-\overline{\nu_\ell}) &= (2.41 \pm 0.22_{\mathrm{stat}} \pm 0.44_{\mathrm{syst}})\%\ . \end{aligned}$$

Acknowledgements

We are grateful to Irinel Caprini, Laurent Lellouch and Matthias Neubert for useful discussions. We wish to thank our colleagues from the accelerator division for the successful operation of LEP. We are indebted to the engineers and technicians at CERN and our home institutes for their contribution to the good performance of ALEPH. Those of us from non-member countries thank CERN for its hospitality.

References

[1] M. Neubert, Phys. Rep. 245 (1994), 259.

[2] H. Albrecht et al. (ARGUS Coll.), Phys. Lett. B 197 (1989), 452. ;
H. Albrecht et al. (ARGUS Coll.), Phys. Lett. B 275 (1992), 195. ;
H. Albrecht et al. (ARGUS Coll.), Z. Phys. C 57, (1993), 533. ;
H. Albrecht et al. (ARGUS Coll.), Phys. Lett. B 324 (1994), 249.

[3] D. Borteletto et al. (CLEO Coll.), Phys. Rev. Lett. 63, (1989), 1667. ;
R. Fulton et al. (CLEO Coll.), Phys. Rev. D 43, (1991), 651. ;
B. Barish et al. (CLEO Coll.), Phys. Rev. D 51 (1995), 1014.

[4] D. Buskulic et al. (ALEPH Coll.), Phys. Lett. B 359 (1995) 236.

[5] P. Abreu et al. (DELPHI Coll.), preprint CERN-PPE/96-011 (1996), submitted to Z. Phys. C.

[6] M. Neubert, Phys. Lett. B 264 (1991) 455.

[7] I. Caprini and M. Neubert, CERN-TH/95-255 (1995), to be published in Phys. Lett. B

[8] D. Decamp et al. (ALEPH Coll.), Nucl. Instr. and Meth. A 294 (1990), 121; ;
D. Buskulic et al. (ALEPH Coll.), Nucl. Instr. and Meth. A 346 (1994), 461;

[9] D. Buskulic et al. (ALEPH Coll.), Nucl. Instr. and Meth. A 360 (1995), 481.

[10] D. Decamp et al. (ALEPH Coll.), Z. Phys. C 53 (1992), 1.

[11] D. Buskulic et al. (ALEPH Coll.), Nucl. Instr. and Meth. A 346 (1994), 461.

[12] D. Buskulic et al. (ALEPH Coll.), Phys. Lett. B 322 (1994) 275.

[13] D. Buskulic et al. (ALEPH Coll.) "Production of Orbitally Excited Charm Mesons in Semileptonic B Decays"
Paper contributed to Warsaw Conference PA01-073

[14] D. Buskulic et al. (ALEPH Coll.), Phys. Lett. B 343 (1995) 444.

[15] A combination of preliminary LEP electroweak Measurements and constraints on the standard model. Draft 2, 1996.

[16] R.M. Barnett et al. "Review of Particle Physics", Phys. Rev. D 54 (1996) 1.

[17] L. Montanet et al. (Particle Data Group), Phys. Rev. D 50 (1994).

[18] H.-G. Moser, "B lifetimes at LEP" talk given in the International Europhysics Conference on High Energy Physics, Brussels 1995.

[19] D. Buskulic et al. (ALEPH Coll.), Z. Phys. C 62 (1994) 179.

[20] Z. Ligeti, Y. Nir and M. Neubert, Phys. Rev. D 49, (1994) 1302.